Searching for Supersymmetry with the α_T variable in $p\bar{p}$ collisions with the CMS Detector at the Large Hadron Collider

Zoe Hatherell

A thesis submitted in fulfilment of the requirements
for the degree of Doctor of Philosophy
to Imperial College London
December 2011

Chapter 1

Theoretical Overview

At the heart of particle physics is a quest to discover the fundamental building blocks of the universe, and how they interact with one another. The field is often given the alternative title "High Energy" physics, as the quest to investigate ever smaller distances as we zoom into the structure of our world is analogous to an increase in the energy scale necessary to view it. Throughout the history knowledge has been advanced through a combination of theoretical postulation using mathematical tools, and experimental searches. Particle physicists seek together to build a full description of the dynamics of the fundamental particles, and while they have discovered much, the picture is not complete yet. The current state of play is collectively known as the Standard Model (SM), and is a rigourously tested and widely accepted theory. However, whilst there are no disagreements, there are some gaps which hint at physics beyond, fuelling a new generation of experimentalists seeking answers to what lies behind.

1.1 The Standard Model

The Standard Model (SM) is the name given to the theories that successfully describes the known elementary particles and their fundamental interactions with respect to the strong, weak and electromagnetic forces. These theories are formulated mathematically using quantum field theory (QFT), in which particles are thought of as excitations of fields, and the dynamics of a given system are summarised in a function called a Lagrangian. In order to reflect the symmetries observed in nature, measurements of physical properties in the SM

must be invariant under local transformations, and this property is called gauge invariance. Therefore the SM is a special case of field theory, called Gauge Theory, and the interactions between particles are described by force-carrying mediation particles known as gauge bosons. From Noether's Theorem, it is known that as a consequence of a symmetry in a dynamical system there is an associated physically conserved quantity. Clearly, for the electromagnetic force this is the electric charge. Analogously, there are conserved "charges" for the strong and weak forces, "colour" charge and the quantum number "isospin", T_3 respectively.

The set of possible transformations is described in the language of Group Theory, and thus we describe the SM as a non-Abelian Yang-Mills type gauge field theory based on the symmetry group $SU(3)_C \times SU(2)_L \times U(1)_Y$. The strong interactions described by Quantum Chromodynamics (QCD) are represented by $SU(3)_C$, and the electromagnetic and weak interactions are represented together due to Electroweak Unification by the group $SU(2)_L \times U(1)_Y$. As of yet, the fourth fundamental force Gravity is not included in the Standard Model, but this is seen as of little consequence as gravitational forces are thought to have comparatively little effect on fundamental particles.

There exist two main types of fundamental particle, which in order to distinguish we must address the concept of spin.

Spin

Spin is the name given to a property of elementary particles, corresponding to a type of angular momentum, although this differs from classical angular momentum. This is an intrinsic property and thus has a specific value for each particle type. The values of the spin quantum number s which describe the magnitude can take any half integer value $s = 0, \frac{1}{2}, 1, \frac{3}{2}$, etc. In addition to magnitude we describe a particle as having spin *up* when the spin is in the direction of the z-axis, and spin *down* if the spin is against the direction of the z-axis. When the spin direction is in the direction of momentum of the particle, it is described as left-handed, and when it is against as right-handed.

All fundamental particles are divided into the spin-1/2 *fermions* which are the building blocks for matter, and the force-mediating *bosons* which must carry integer spin, usually spin-1.

The fermions which make up all visible matter can be described in three

families, or "generations", shown in Equation 1.1. Within each generation, there are two sets of particles, those on the left are the leptons, which interact by the weak and electromagnetic forces only, and those on the right are the quarks, which also interact by the strong force. In each generation, there are two quarks, which differ by electoral charge - one has +2/3 and the other -1/3 (in units of the electron charge e), an electrically charged lepton and a neutral lepton called a neutrino which is either massless or very light. The three families then are organised in ascending order of mass. The first generation is therefore stable and all ordinary matter is constructed from it, whilst the second and third are liable to decay into particles of the first generation. In addition to each particle detailed here there exists a corresponding antiparticle due to a symmetry in charge and quantum numbers.

$$\begin{bmatrix} \nu_e & u \\ e & d \end{bmatrix}, \begin{bmatrix} \nu_\mu & c \\ \mu & s \end{bmatrix}, \begin{bmatrix} \nu_\tau & t \\ \tau & b \end{bmatrix} \tag{1.1}$$

The particles which mediate the forces are bosons, the photon γ for the electromagnetic force, the 8 gluons g_i for the strong force and the $W^\pm$ and Z bosons that carry the Weak force, all of which are spin-1 particles. The final particle of the SM is the Higgs Boson of spin-0, as yet undiscovered in experiment but expected from the theory, as we will see later.

1.1.1 Gauge Theory of Interactions

Everything in our Universe interacts by way of gauge bosons mediating one of the four fundamental forces. Whilst the SM incorporates the electromagnetic, strong and weak forces, it as of yet has not been possible to describe the gravitational force in this way.

Quantum ElectroDynamics

The fundamental electromagnetic force is studied in quantum field theory as Quantum Electrodynamics (QED), the oldest and simplest of the theories brought together to form the SM. The symmetry of QED is U(1) and this gives an associated conserved quantity, the electric charge Q. The electromagnetic force is carried by the massless boson, the photon, and affects only the charged fermions.

The symmetry allows no self interaction of the photon. The fermion field ψ_q with charge q and mass m_q gives rise to the Lagrangian in Equation 1.2.

Lagrangian

$$\mathcal{L}_{QED} = \bar{\psi}_q(i\gamma^\mu \not{D}_{QED,\mu} - m_q)\psi_q - \frac{1}{4}F_{\mu\nu}F^{\mu\nu} \tag{1.2}$$

Here, $\not{D}_{QED,\mu}$is the covariant derivative, incorporating the introduction of a photon gauge field A_μ, so as to maintain an invariance to local U(1) charge symmetry. Thus,

$$\not{D}_{QED,\mu} = \partial_\mu + iQA_\mu \tag{1.3}$$

where Q is described as the generator of the symmetry group and is analogous to electric charge. The strength of coupling of each force is described by the coupling constant, in this case governed by the constant e, the charge of an electron: $\alpha = \frac{e^2}{4\pi}$

QCD

Quantum Chromodynamics (QCD) is the relevant quantum field theory that describes the dynamics of the strong force. The strong force of symmetry group $SU(3)_C$ has 8 massless gauge bosons known as the gluons, and a conserved quantity called colour charge, which has three types called $q_i i = 1, 2, 3$. The name "colour" is not meant to imply a connection to visual colour, merely an analogy between the three types and the primary colours red, blue and green. Only particles which carry colour charge are affected - the quarks have colour, while leptons do not. Unlike the photon in electromagnetism, the gluons that mediate the force carry the charge also, leading to the self-interactions that govern the behaviour of QCD.

A quark carries one "colour" q_i, taking one of the three possible values, and an analogous antiquark carries one "anti-colour". On the other hand, gluons carry both a colour and an anti-colour. Separation of two charges gives rise to a potential energy, which increases linearly as the charges are moved further apart. As a consequence, it would take an infinite amount of energy to separate two quarks, and thus they are not found free in nature, but only bound within colourless hadrons such as the proton p $\sim$ uud and the neutron n $\sim$ dud, an effect we call *confinement*. This explains why colour charge is not observed in nature,

as beyond a fundamental level it has no meaning.

To describe this behaviour, the coupling constant of the strong force, α_S as the distance between two particles is increased, or as the energy scale is increased, in comparison to the coupling constant for QED which has the inverse relationship. When we discuss quarks in particle physics although they are free, this is as a result of the "asymptotic freedom" where when viewed at very large energies the distances are infinitely small, and the quarks behave freely. tat

$$\mathcal{L}_{QCD} = \sum_q \bar{q}(i\gamma^\mu \not{D}_{QCD,\mu} - m_q)q - \frac{1}{4}F^\alpha_{\mu\nu}F^{\mu\nu}_\alpha \tag{1.4}$$

The Weak Force and Electroweak Unification

The weak interaction, responsible for radioactive decay, makes up the final piece of the puzzle. So named because of its comparatively low strength compared to the electromagnetic and strong forces, it is was theorised as being mediated by massive force bosons $W^\pm$ and Z long before they were discovered experimentally. A lagrangian theory for the weak force must take into account the characteristics of weak interactions. Firstly, it is capable of flavour changing in quark interactions. Secondly, it shows a chirality whereby it interacts with only left-handed fermions, and right handed anti-fermions, violating Parity, P. It also violates ye Thirdly it is capable of both charged interactions which violate the charge C, and neutral interactions which do not. Whilst C and P can both be violated, the product CP

describing the interactions of the left-handed fermion doublets. The group symmetry is SU(2) giving rise to a conserved quantity known as weak isospin, I. Building an individual Lagrangian to describe the picture of weak interactions was not as simple as in the strong and electromagnetic sectors, with each proposed model suffering problems. Finally it was realised that despite their apparent differences the weak and electromagnetic forces were low-energy manifestations of the same force, and a composite theory was proposed [1]. This is called Electroweak Unification, and for this the Nobel Prize was awarded to Glashow, Salam and Weinberg in 1979 [2].

The gauge group of the unified theory is $SU(2)_L \times U(1)_Y$, where $U(1)_Y$ is a different copy of the symmetry seen in electromagnetism, the $U(1)_{em}$ group. In this picture the conserved quantity is Y, the weak hypercharge, and the conserved

quantity for the SU(2) symmetry is the weak isospin, T_3. The previous quantity conserved under $U(1)_{em}$ Q can be defined as a linear combination of the two $Q = T_3 + \frac{Y}{2}$. The $SU(2)_L$ suffix is not taken from the conserved quantity, T_3, but from it most important property, its action on only Left Handed (LH) fermions. Fermions that are Right Handed (RH) have a weak isospin $T_3 = 0$ and do not interact via the weak force, whereas LH fermions have $T_3 = \pm\frac{1}{2}$ and interact via three gauge bosons. The $W^{\pm}$ bosons have each an isospin of unit 1, with a sign defined by the name, and they govern an interaction from a particle of $T_3 = +\frac{1}{2}$ into one of $T_3 = -\frac{1}{2}$ and vice versa, according to conservation laws. The third boson given by the SU(2) group alone is the W^0 boson of $T_3 = 0$, which allows interactions where the weak isospin stays the same. This is not a physically observed particle, as the electroweak unification leads to mixing between this and the boson given by the $U(1)_Y$ group to produce the photon and the Z^0 particle.

1.1.2 EWSB and the Higgs Mechanism

In order to give mass to the W and Z bosons whilst retaining the necessary local gauge invariance, we say that $SU(2)_L \times U(1)_Y$ must be spontaneously broken into $U(1)_{em}$, the group of symmetries representing the electromagnetic sector. The simplest way to introduce such a breaking is known as the Higgs Mechanism, and corresponds to the addition of a scalar field. Ensuring the change to the Lagrangian is invariant, there is a covariant derivative term and an additional potential. With the construction of a potential colloquially known as a "mexican hat" potential [NEEDPIC], the minimum does not lie at $\phi = 0$, but in 3D space in a circle of minima around ϕ, so there are an infinite number of minima, introducing a degeneracy. As a particular vacuum is chosen, the symmetry is broken. Interactions with the field lead to masses for the W and Z bosons. This leads to the existence of a massive scalar particle, known as the Higgs Boson, to date the only particle of the SM yet to be observed.

The distinction between the two forces caused by this symmetry breaking are due to a linear combination of the weak hyper charge and isospin, T_3 and Y that vanishes for the Higgs. As this defines the conserved quantity Q for the electromagnetic group, this is not affected by the higgs, and thus the $U(1)_{em}$ group remains unbroken. Conversely, the weak portion interacts with the Higgs and the W± and Z bosons acquire mass.

1.2 Motivation for Physics Beyond the Standard Model

The standard model has been widely successful, predicting the existence of particles such as the $W^{\pm}$ and Z Bosons, and the t quark, showing impressive agreement with experimental findings at the level of 0.1%. However, there are several signs that it is not a complete theory, that more information is needed to describe physics at higher energy scales. It can be assumed that the Standard Model is a low-energy .

The SM does not currently incorporate the gravitational force, a problem which has not bothered particle physicists much as the strength of the effects of gravity on fundamental particles is negligible compared to the other fundamental forces. However, at an energy known as the Plank Scale, $M_p \sim 1{-}^{18}$ GeV quantum gravitational effects become important, leading to the breakdown of the existing QFT picture of the Standard Model. Thus new physics must exist at this energy scale, or before, indicating the SM is only valid up to some unknown energy scale. Several other theoretical problems exist motivating theories for physics Beyond the Standard Model (BSM) at the TeV scale, which we are able to explore for the first time with the LHC.

nor does it explain the existence of dark matter and dark energy. Neutrino masses and flavour mixing are also unexplained. In addition, several features of the existing SM are seen as inelegant, as they require some mathematical fine-tuning and thus are unlikely to reflect nature. The main motivations for

1.2.1 The Hierarchy Problem

Although the Higgs Boson has yet to be observed experimentally, its mechanism is necessary to the Standard Model to provide mass to the particles, and thus is considered to exist unless proven otherwise. However, while it solves the SSB problem, the Higgs theory introduces theoretical issues of its own. The presence of the Higgs in the SM ensures the WW scattering amplitude does not violate unitarity, but only whilst the $m_H < 1TeV$, providing an upper bound on the expected mass[3].

However, in the coupling of the Higgs to heavy fermions, the mass of the Higgs receives extremely large radiative corrections. If each coupling with a fermion f

has a term in the Lagrangian $-\lambda_F H\bar{f}f$, it contributes a quadratically divergent factor δm_H^2 that corrects the squared mass of the Higgs.

$$\delta m_H^2 = -\frac{|\lambda_f|^2|}{8\pi^2}\Lambda_{UV}^2 \tag{1.5}$$

The parameter Λ_{UV} is the *ultraviolet cutoff*, so named as it represents the smallest distance to probe in the calculation. It can be thought of as the scale at which the Standard Model is valid up to, as any new physics would change the theory. If there were no new physics at a lower energy, it takes the value of the Plank Scale M_P, but in this case the correction will be 30 orders of magnitude higher than the 1 TeV upper bound justified experimentally. As there exists nothing in the SM to fix the Higgs Mass, the theory requires fine-tuning, tweaking the parameters to agree with observational findings. This is generally accepted to be an inelegant method, as it requires the input of extra information, and indicates a gap in the fundamental description leading to searches for extensions to the Standard Model.

1.2.2 Cold Dark Matter

The existence of Dark Matter was postulated as early as 1933 by Zwicky [4], as the orbital velocities of galaxies in clusters were inconsistent with their observed mass, suggesting some additional mass was present but not luminous. Measurments of rotation curves of galaxies, cosmic microwave background and structure formation have confirmed this concept over the years. Experimental results from WMAP conclude only $\sim$ 4.5% of the energy in our universe is made of the baryonic matter we see, while dark matter accounts for $\sim$ 23% and the rest is comprised of another unknown, dark energy. Although the existence of such matter has been well documented, there is still no understanding of the physics behind the phenomena. In order to explain the properties a weakly interacting massive particle (WIMP) is required, and it must be electrically neutral. There is no provisions for such a particle in the SM, indicating additional particle content requiring extensions in the theory.

1.2.3 Unification of Coupling Constants

At the basis of theoretical particle physics is the observation of the symmetry and simplicity of nature. Unification, where several theories can be combined into one description, has undergone before, first Electricity and magnetism, and then electromagnetism with the weak force. While each of the three forces of the SM have their own coupling constant, as the energy scale is increased the coupling constants converge towards one another. However precision measurements show that within the current framework, there is no common point where all three intersect. In addition, at the Planck Scale as gravity's coupling constant would be of similar strength many hope for a Grand Unified Theory (GUT), occurring at this scale known also as the GUT scale. This is only possible with the incorporation of some new physics which would alter the trend of the couplings between the electroweak scale and this GUT scale.

1.3 Supersymmetry

The hierarchy problem could be removed, rather than controlled, if there were a way to cancel out the quadratic diverging term in the Higgs mass correction. As the correction for bosons has the opposite sign, the conception of a new symmetry was born, one between fermions and bosons. Known as SUperSYmmetry (SUSY), this theory extends the SM under this symmetry such that elementary particles in the SM each have a super partner differing by one half unit of spin as yet undiscovered, just as the anti-particles were once postulated. For every fermion contributing to the quadratic divergence, a boson partner contributes the equal and opposite term, and thus the hierarchy problem cancels out and the mass of the higgs can take a sensible value.

Under this symmetry elementary particles in the SM would each have corresponding super-partners, differing by one half unit of spin, such that a fermion has a scalar boson super partner, and vice versa. At the heart of supersymmetry is a transformation that changes the field of a fermion into that of a boson, and vice versa. The generator of the transformation shall be known as Q,

$$Q|fermion>=|boson>, Q|boson>=|fermion> \tag{1.6}$$

According to an exact symmetry a super partner would have the same characteristics as its partner, including its mass, which would indicate they were within the reach of previous physics experiments. However, they have not been observed, and thus it is concluded that the symmetry is broken at some energy scale, to give the superpartners greater mass. In order for SUSY to eliminate the hierarchy problem, this breaking is assumed to occur at the Electroweak Scale, which restricts the size of the difference in mass to the order of 1 TeV. This is known as "soft" SUSY breaking, and offers the hope of discovering this new physics at the TeV scale, as is now possible for the first time with the LHC.

In addition to its neat solution to the hierarchy problem SUSY has several other consequences which lead to its position as the most favoured theory for new physics at the TeV scale. The inclusion of SUSY particles to the SM has the side affect of altering the runnings of the gauge coupling constants of the three fundamental forces, discussed above, such that they are consistent with theories of Grand Unification, an energy scale at which the three are equal. Rather than a motivation, this is a pleasant coincidence, but lends plausibility to the theory. It also shows promising features necessary for theories to incorporate gravity, although it does not finish the job. SUSY itself cannot be the final fundamental theory of particle physics, but is an extension which shows much promise. The final, perhaps most exciting feature of SUSY is that it can offer a candidate for the particle that represents dark matterm with the introduction of a new quantum number R - Parity.

1.3.1 R-Parity

Consructing the most general form of SUSY, terms appear which allow processes which violate two quantum numbers, the baryon number B and the lepton number L. Whilst there is no theoretical reason for this to be a problem, these interactions have not been observed, and are constrained heavily. An undeniable constraint is the lifetime of the proton, which is very large, whereas these processes would facilitate its decay. whilst B and L are not fundamental symmetries in the theory, it is possible to construct a new quantum number R defined in Equation 1.7 which can be required as a symmetry R-parity. It distinguishes between particles from the SM and the sparticles introduced by SUSY, as under this construction, all SM particles carry R of +1 and all super partners carry -1.

$$R = (-1)^{3(B-L)+2S} \tag{1.7}$$

Whilst terms in the Quantum Field Theory do allow for the possibility of violation of this parity, experimental measurements has excluded this for sparticles with masses on the TeV scale, and therefore those within the reach of the LHC. Thus the majority of searches consider models with a symmetry which forbids this violation and conserves Rp. Several phenomenological consequences arise from this assumption which provide the backbone to SUSY searches at the LHC.

IN over for SUSY particles to be produced at the LHC under this framework, they must be pair produced from SM particles. The heavier particles undergo a decay chain ending in the lightest of the supersymmetric particles, denoted the Lightest Super Partner (LSP), and this particle is by necessity stable and neutral, as it cannot decay into SM particles. These characteristics denote it a WIMP, the type of particle that is sought in Dark Matter searches. These particles will not interact in a detector, therefore are characterised in an experiment as large amounts of missing energy. As this is directly a characteristic of a WIMP in the final state, such a signature represents not only SUSY but is shared by other new physics models with a dark matter candidate particle.

Models may be constructed to constrain the violation of B and L without R-parity conservation, but those shall not be considered in this thesis, as this unique feature provides both physical motivation and a search strategy for physics at the LHC.

1.3.2 MSSM

Whilst there are money ways to construct mathematically the theory of Supersymmery, it is usual to do it in the way which introduces the least number of new degrees of freedom. This corresponds to the minimal particle contact required to satisfy the core symmetry, which corresponds to one new degree of freedom for each existing SM one. This approach is known as the Minimal Supersymetric Standard Model (MSSM), and has an additional new particles, known as a sparticle, for each known SM particle.

The particles are arranged to fit the irreducible representation of the symmetry, in *supermultiplets*, each of which contains both fermions and bosons.

The number of bosonic and sermonic degrees of freedom are therefore equal in any supermultiplet. The names of the spin-0 bosons that partner the SM fermions are prepended by "s", known as squarks and sleptons, collectively the sfermions.

The Higgs receives different treatment in SUSY, as not one but two Higgs supermutiplets are required, to give mass separately to the quarks of charge ⅓ and the quarks of charge ⅔

1.3.3 Minimal Supergravity and the Constrained MSSM

Even assuming a minimal particle content, the MSSM has a large number of free parameters, introduced through SUSY and Electroweak symmetry breaking, 105 more than the SM. When it comes to experimental searches, this is an unworkable number, for to examine possible behaviour of SUSY one would have to look in 105 dimensions. Thus for the purpose of making models to work with, it is desired to constrain this number in the theory. One popular theory used in this thesis is the theory of minimal SUper GRAvity, otherwise known as mSUGRA.

The concept behind mSUGRA is that there should be some messenger between the MSMM sector and

Current Limits on the CMSSM

Two types of limits exist in mSUGRA space, those imposed theoretically and those that result from experimental data. Of the latter, some are contributed from cosmology, and others from particle physics.

There are some regions of th parameter space where the masses of the particles have a hierarchy which results in the stau being the LSP. This is theoretically forbidden as the LSP certainly contributes some if not all of the dark matter in the universe, and it is known to be neutral.

1.3.4 Other BSM Models

1.3.5 Production Mechanisms at the LHC

The Parton Model

Chapter 2

The Compact Muon Solenoid Experiment at the LHC

2.1 The Large Hadron Collider

The Large Hadron Collider (LHC) is a double-ring circular synchrotron at CERN designed to collide two proton beams with a centre of mass energy $\sqrt{s} = 14$ TeV at a final design luminosity of $10^{34}\text{cm}^{-2}\text{s}^{-1}$. The energy and luminosity have been chosen to with the aim of discovering new physics at the TeV scale, out of reach to previous experiments, where theories predict new physics both within and outside the Standard Model. It will also be used to collide heavy lead ions (Pb^{82+}) to an energy of 2.76 TeV per nucleon, in specific runs, with the purpose of investigating QCD matter at energies 30 times higher than previous experiments. The LHC has unparalleled reach in the search for new physics, not only due to the significant increase of energy over the Tevatron, the previous record holder, but also due to the intensity of the beam delivered. The number of events produced by a given physical process depends proportionally on its cross section σ, and therefore proportional to $\sqrt{s}$ and the luminosity $\mathcal{L}$, which has the dependence shown in equation 2.2 below [5]:

$$n = \mathcal{L}\sigma, \qquad \mathcal{L} = \frac{N_b^2 n_b f_{rev} \gamma_r}{4\pi\epsilon_n \beta^*} F \tag{2.1}$$

where N_b is the number of particles in a single bunch, n_b is the number of bunches in a beam, f_{rev} the frequency of revolutions, γ_r is the relatavistic gamma,

ϵ_n is the beam emittance and β^* is the beta function associated with the collision point. The geometric luminosity function F provides a reduction factor based on the beam crossing angle, and depends on the full crossing angle at the IP θ_c, and the transverse and longitudinal RMS beam dimensions σ_* and σ_z with the following dependency:

$$F^2 = \frac{1}{1 + (\frac{\theta_c \sigma_z}{2\sigma_*})} \tag{2.2}$$

Situated in the tunnel of the previous e^+e^- machine LEP located underneath the Franco-Swiss border, the LHC is mostly circular with a circumference of 27km, consisting of 8 arced sectors connected by 8 straight sections in which are the numbered Interaction Points (IP), where the two beams circulating in opposite directions can be allowed to intercept. To bend the protons around the rings, the beams must experience opposite dipole fields from one another, and have two separate vacuum systems. As the tunnel has restricted space available, the dipole magnets are twin bore with two coils and, but share the same structure and cryogenics. The 1232 superconducting dipole magnets present must produce a field in excess of 8T due to the high momentum of the protons, and thus have a high current and must be cooled below 2K by liquid helium to ensure safe operation. The beams are non-continuous, grouped in "bunches" at intervals. In the straight sections the two beams share the same beam line and can be directed to coincide at the IP's. In order to maximise the number of interactions, quadropole magnets are used to collimate the beam providing a minimum cross section at the moment of interaction.

At four of these IP's are located the four main detectors that analyse the data from collisions: the two high luminosity experiments ATLAS (A Toroidal LHC Apparatus) at IP1 and CMS(Compact Muon Solenoid) at IP5 are multi-purpose detectors analysing the p-p collisions for signs of new physics. At IP8 the LHCb (LHC beauty) detector looks for CP violation and other rare decays in a forward detector with lower luminosity runs, and ALICE (A Large Ion Collider Experiment) at IP2 will investigate the lead-lead ion collisions. The locations of the detectors in the LHC ring is shown in Figure 2.1 [6] .

The magnets are optimised for beams of a certain energy range, and therefore the protons cannot be fully accelerated in the LHC. Therefore supply of protons are delivered through a series of other machines that make up part of the CERN accelerator complex, the layout of which is shown in Figure 2.2.

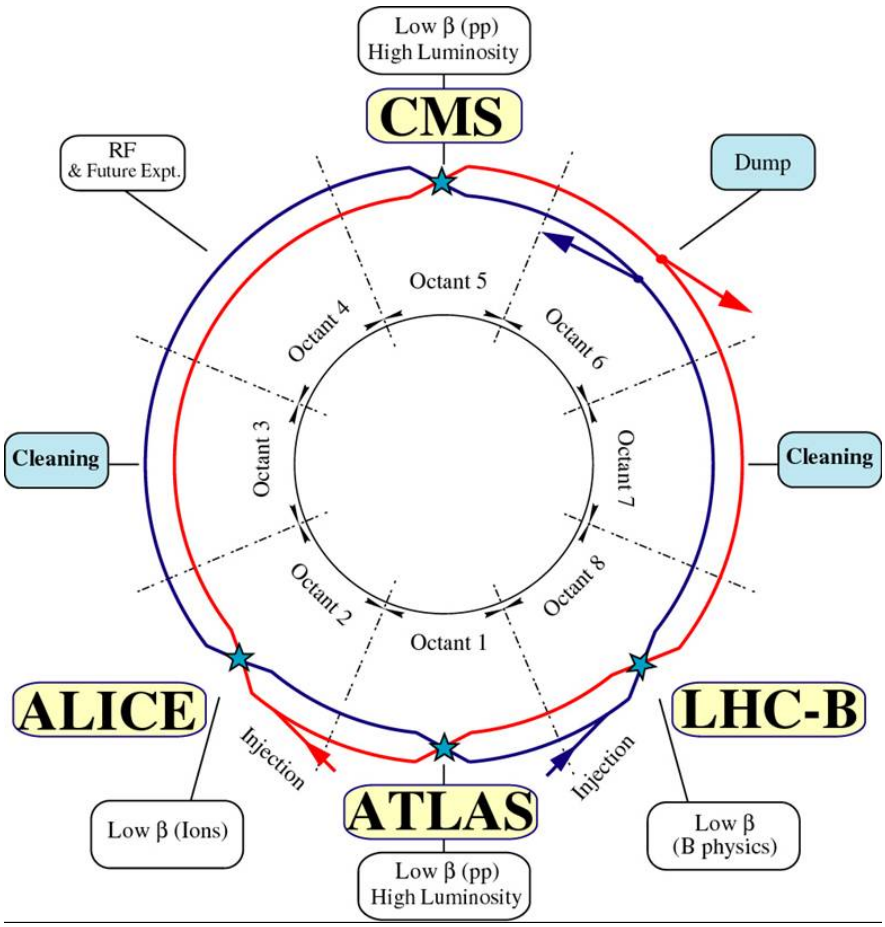

Figure 2.1: Schematic of the LHC ring and the location of the major experiments.

A beam of 50MeV protons is created in LINAC2, in 6 bunches, and each bunch is then split into 12, resulting in 72 bunches which are fed into the Proton Synchotron Booster. After accelerating to an energy of 1.4GeV, they enter the Proton Synchotron, where they are accelerated to 26GeV, and fed in sets of 2-4 into the Super Proton Synchotron. Now 144-288 bunches, they are accelerated to 460GeV ready of injection into the LHC. Twelve of these sets are injected into the LHC at one, directly into both rings, giving a nominal bunch density of 2808, with a spacing of 25ns. This process takes around 20 minutes, and then the LHC takes a further 20 minutes to ramp the protons up to the desired energy. The magnets preventing the beams coinciding in the detectors are turned off and stable collisions occur. However, the luminosity falls regularly as the run progresses, and after 6-12 hours, it has fallen below an acceptable level, and the beam is dumped before repeating the process again.

Using these short runs of high luminosity it is possible for the LHC to take vast amounts of data, and assuming 200 days of data taking a year at design luminosity the machine will be able to deliver 100fb^{-1} a year. As part of the early phase of operation the machine was operated in 2010-2011 at 3.5 TeV per beam, $\sqrt{s}$ =7TeV, in order to protect the magnets, and is not expected to run at full energy until 2014. The 2011 run delivered 5.727fb^{-1} data, the first 1.1fb^{-1} of which was delivered by the end of June, and is considered for this thesis.

2.2 The Compact Muon Solenoid

The Compact Muon Solenoid (CMS) is one of the two high-luminosity multi-purpose detectors at the LHC, designed to capitalise on the full range of physics opportunities available as a new energy scale is probed. These goals are pursued through the design and construction of the detector and development of software for the reconstruction of physics objects. The detector is constructed of several detector sub-systems contained inside and wrapped in layers around a central 13m long 4T super conducting solenoid as shown in Figure 2.3.

The detector is 21m long, 15m wide and weighs 14000 tonnes, and consists of five wheel-like barrel sections and two end-caps to close. In order for CMS to search for new physics among the high order of Standard Model backgrounds, it is of key importance to develop a detector which has impressive energy and

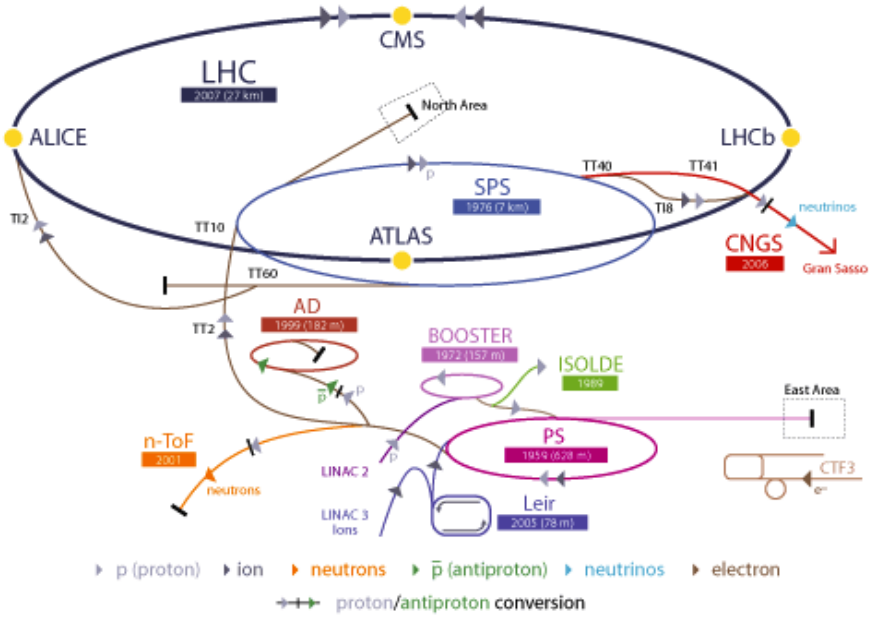

Figure 2.2: Layout of the CERN accelerator complex, illustrating the relationship between the LHC and its supporting accelerators tasked with delivering proton beams at 460GeV.

momentum resolution, and particle identification. Different particles interact differently with matter and therefore a number of sub-detectors are needed in order to gather all the relative information. This is then combined in order to reconstruct the objects.

The high magnetic field was chosen in order to achieve the bending power necessary for good charged particle momentum resolution. The inner bore of the solenoid is large enough that the inner tracker and the calorimeters are located inside, which minimises the material the partials pass through before entering the calorimeters. This allows a good energy measurement. Four muon "stations" of aluminium drift tubes are integrates within the iron magnetic field return yoke. The full design description can be found in the CMS Technical Design Proposal [7]. As different particles pass through the detector they interact in the sub-systems depending on their type. A transverse slice through the detector illustrating the path through the machine of each type of particle is shown in Figure 2.4

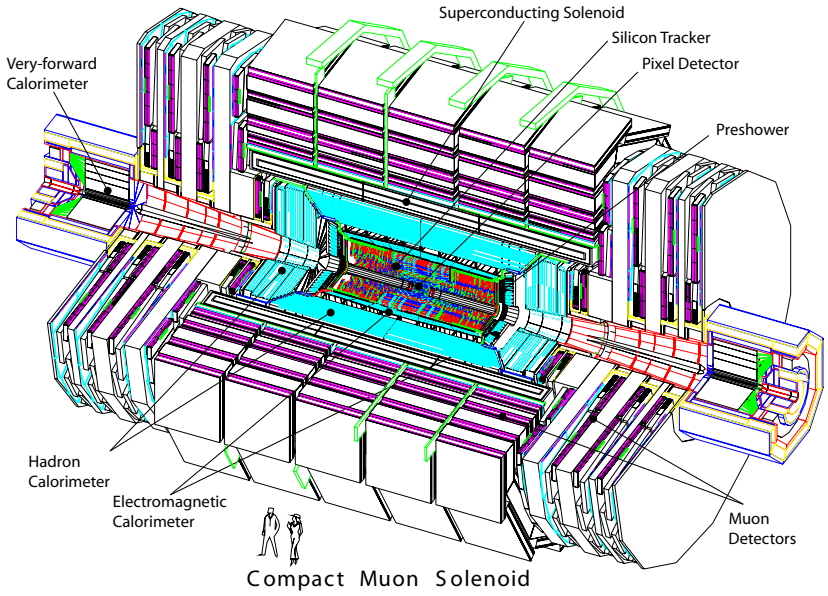

Figure 2.3: A cutaway diagram of the CMS detector structure identifying the main individual sub-systems.

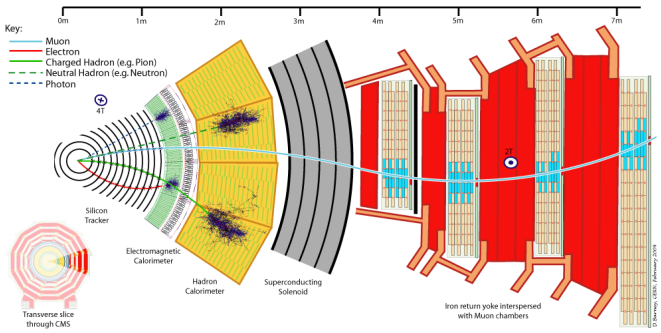

Figure 2.4: Transverse slice through the CMS Detector showing each type of particle and how it interacts with the sub-detectors.

2.2.1 Coordinate System

The coordinate system chosen by CMS uses the nominal interaction point within the detector as the origin. The x-axis points radially inwards to the centre of the beam pipe, and the y-axis points vertically upward. The z-axis then points in the direction of the beam. The azimuthal angle ϕ is defined as the angle from the x-axis in the x-y plane, and the polar angle θ from the z-axis. However, it is common convention to express θ in terms of the Lorentz Invariant quantity, pseudorapidity $\eta = -\ln\tan(\theta/2)$, as particle production is approximately uniform in η. The transverse components of the energy and momentum, denoted E_T and p_T are then calculated form the x and y components.

2.2.2 Superconducting Magnet

The geometry of the magnetic field is integral to the design and cylindrical structure of the CMS detector, as it uses a global solenoidal magnet. A strong magnetic field is essential to the design of a detector, bending charged particles in order to measure their charge and momentum. In order to ensure that the curvature is significant even with particles of high momentum, the CMS solenoid is designed to be capable of delivering a homogenous field of 4T. Consisting of four layers of NbTi coils, in a vacuum with a cryogenic system maintaining a temperature of 4.5K, the solenoid has a diameter of 5.9m and length 12.5m, and when operating at full current is cable of storing 2.6 GJ of potential energy.

As the solenoid is so large, not only the inner tracking system but also both calorimeter sub-detectors can be accommodated in the interior, giving significant advantage to electromagnetic and jet energy resolution as particles will not have traversed the high-density magnet coil before these measurements are taken. The flux is returned with a large iron yoke of $10^7 kg$, surrounding the inner magnet and built with a barrel of 5 wheels, and two end-caps each containing three disks. The muon system is built within the iron return yoke, in order to take advantage of the reverse magnetic field produced in the outer region, and thus follows the same structure. The drawback of a solenoidal field is that it had strong inhomogenity in the end-caps, affecting the performance of the muon subsystem, which shall be discussed later.

2.2.3 Tracker

The first sub-detector encountered by particles is the multi-layer silicon tracker, which records precise information about the path of charged particles bending under the magnetic field. It is placed as close to the interaction point as possible in order to distinguish the primary interaction from secondary vertices of particles with significant lifetimes. This is particularly important in the case of identifying B mesons, which can travel a measurable distance before decaying.

The tracker is divided into regions defined by the radius r from the interaction point, as the expected particle flux decreases rapidly as the radius increases. This is due to the high magnetic field, which causes low momentum particles to have small radial helical trajectories.

Nearest to the primary vertex at 4cm, where the expected particle flux is at its highest ($\sim 10^8 cm^{-2} s^{-1}$) are 66 million silicon pixel detectors of size 100 $\times$150 μm^2, arrayed in three barrel layers and two end-cap disks. This region is laid out to optimise the resolution in determining the vertex position, delivering a granularity of $10\mu m$ in the r-θ plane and $20\mu m$ in the r-z plane. Pixel detectors have the advantage of being able to measure all three coordinates of the particle simultaneously. However this requires a huge number of readout channels and drives the costs of construction up. For this reason these are chosen for the innermost region where the flux is highest, while the test of the detector are composed of silicon micro-strip devices.

Outside of the pixel detector lies the silicon strip tracker beginning at r = 20cm, divided into two parts, the inner and outer components. As the flux of particles expected is lower than in the pixel detector, the use of 11.4 million silicon strip detectors allows the deserted granularity while reducing costs. Whilst these do now allow a simultaneous 3-coordinate measurement, the layers are constructed at known angles to one another and therefore combined together all three coordinates can be measured. The inner region, immediately outside the Pixel tracker, is composed of four barrel layers (TIB) and closed with three disks (TID) on each end, occupying the region up to r=55cm, where the microstrip sensors are 320μm thick oriented along the beam line in TIB and radially in the TID. The outer region has 6 barrel layers (TOB) further apart than in the inner sector, and closed with 9 end-caps (TEC) on the end of the barrel, extending out to r=116cm. The strips here are 500μm thick

In total the tracker covers a total area of 205m^2 with 76 million channels and provides a transverse momentum measurement for high momentum tracks with resolution 1-2% in the region $|\eta| < 1.6$.

2.2.4 ECAL

Immediately outside of the tracker, and still within the magnet core, sits the Electromagnetic Calorimeter (ECAL), used to measure the energy of electrons, photons and pions via the energy they lose through radiation. Electrons lose their energy in the material through bremsstrahlung, and photons by decaying to an electron-positron pair. Using a hermetic homogenous calorimeter of scintillating crystals, this energy can be converted to scintillation light which is picked up by a light sensitive detector.

The use of high density crystals allows a fast calorimeter which has fine granularity and is radiation resistant, requirements which are essential in the LHC environment. After rigorous research and development, lead tungstate ($PbWO_4$) crystals were chosen as the optimal solution to the requirements of LHC operation, due to a number of desirable characteristics. The extremely short radiation length $X_0 = 0.89$cm allows the construction of a compact ECAL which therefore can reside within the solenoid, hence reducing the layers of material the particles have already passed through. In addition, the material has a low Moliere radius (2.2cm) meaning the transverse size of the electromagnetic shower is small, leading to good shower position resolution and separation. It is also essential that a fast scintillator is used, in order to distinguish between bunch crossings. In crystals of $PbWO_4$ 80% of the scintillation light is emitted within 25ns, the bunch spacing of the LHC. Finally the crystals are hard to radiation, as their method of scintillation is resistant to radiation damage.

The ECAL is structurally divided into three distinct regions, the End-caps (EE), the Barrel (EB) and the Preshower (PS), which together cover a pseudorapidity range $|\eta| \leq 3$. The ECAL Barrel is a cylindrical arrangement of 61200 $PbWO_4$ crystals covering the pseudo rapidity range $|\eta| \leq 1.479$ with a granularity of $\Delta\eta \times \Delta\phi = 0.0174 \times 0.0174$. The radius to the front-face of the crystals is 1.29 m.

The ECAL is closed by two identical end-cap regions, which cover the range $1.479 \leq |\eta| \leq 3$ at the margins of the barrel, each consisting of 7324 crystals

divided into two halves, or *Dees*. Precision energy measurements are possible up to $|\eta| = 2.6$, but crystals are include up to $|\eta| = 3$ to assist the forward-direction energy-flow measurement. The end cap crystals are also wedge shaped with a square front face $28.62 \times 28.62mm^2$ and a square back face $30 \times 30mm^2$. The crystals point slightly away from the interaction point in order to make the end-caps hermetic, and are grouped mechanically into 5×5 super-crystals (SC).

The size of the crystals is chosen to reflect the properties and requirements, such that the front face surface area is 22mm x 22mm (the size of the Moliere radius) and the longitudinal depth of the crystals is 230mm, which is 25.8 X_0 in the barrel, hence allowing a fine granularity and a compact ECAL. In the end-caps the presence of the PS allows for shorter crystals, of 220mm, corresponding to 24.7 X_0.

A additional component, the Pre-Shower is present in front of the end-caps covering a range of $1.653 \leq |\eta| \leq 2.6$ and consists of two layers of absorbing lead converters and silicon detectors. The primary function of the PS is to identify neutral pions that decay into two photons in the end-caps, which can fake a high-energy photon. It also possesses a high granularity, and therefore is used to improve position determination of particles, and helps the identification of electrons against minimum ionising particles. The two layers of the PS have their strips orthogonal to one another such that the first layer has vertical strips to measure the critical position, and the second horizontal strips for the horizontal position.

The scintillators are read out using photodetectors, which convert the scintillating light of the crystals into an electric signal. The crystals were chosen by a rigorous optimisation of the properties required, which results in a high-performance ECAL, however this material has a relatively low light yield. In order to overcome this, photodetectors designed for use in a magnetic field with intrinsic gain are used. Vacuum Phototriodes (VPTs) are used in the end-caps. These are unsuitable in the central region due to high magnetic, but due to lower radiation levels Avalanche Photodiodes (APDs) are used. Both the crystals and the photodetectors are sensitive to temperature changes, so a stable temperature must be maintained. Radiation damage to the crystals decreases with temperature, but so do the thermal effects which result in recovery. The operational temperature, 18C is chosen as it is the point of equilibrium between

damage and recovery.

The resolution of an ECAL can be described as a function of the energy E in GeV, shown in Equation 2.3, for energies below about 500 GeV [8]. Above this shower leakage from the back of the crystals become non-negligible.

$$\left(\frac{\sigma}{E}\right)^2 = \left(\frac{S}{\sqrt{E}}\right)^2 + \left(\frac{N}{E}\right)^2 + C^2 \tag{2.3}$$

The stochastic term S represents fluctuations related to statistics, including photoelectron statistics and intrinsic shower variations. The noise term N takes into account electronic noise summed over readout channels, and the constant term C accounts for the uncertainty in calibration and the detector non-uniformity. Measurements from test beam reconstructed energy distributions show values for the terms to be $S = 2.8 \pm 0.1\,\%$, N=0.12 GeV and $C = 0.30 \pm 0.01\,\%$.

2.2.5 HCAL

Outside the ECAL lies the Hadronic Calorimeter (HCAL), responsible for the measurement of the hadronic activity of an event. This also leads to a measurement of apparent missing energy from neutrinos or exotic particles, an important quantity in many searches for new physics. In order to measure the energy of hadrons in a compact space, a sampling calorimeter of interleaved layers of absorbers and scintillators is used. The absorbing material forces hadronic showering through nuclear interaction with heavy nuclei, and the active scintillating material then detects samples the showers of charged particles produced. The absorber material is described by the interaction length λ_I, the distance a hadron will travel through the material before it has lost roughly 63% of its energy through nuclear interactions.

The HCAL is divided into several sections, defined by pseudo-rapidity in order to optimise the resolution under different conditions. Within the space between the ECAL and the magnet coil lie the HCAL Barrel (HB) at $|\eta| < 1.305$, and the HCAL End-Caps (HE) at $1.305 < |\eta| < 3.0$, hermetically joined to completely surround the ECAL. In order to increase the hermicity of the HCAL, and therefore improve the accuracy of the missing energy measurement, the two elements of the HCAL Forward calorimeter (HF) overlap with the HE and extend the range in pseudorapidity to $|\eta| < 5$. There is also a complimentary layer

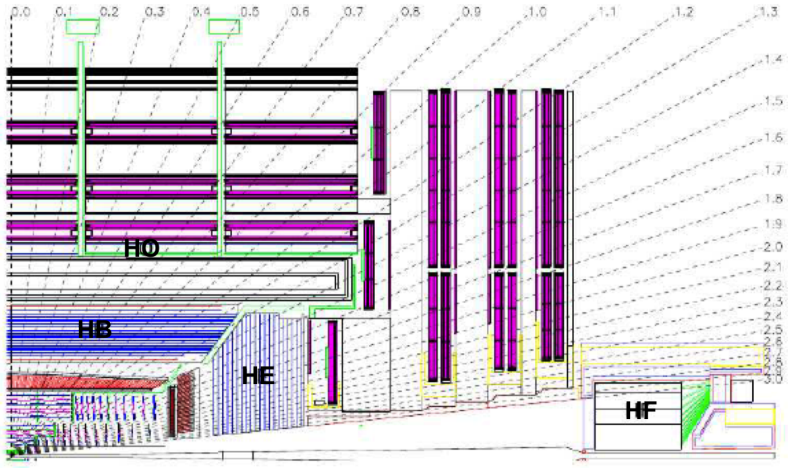

Figure 2.5: Diagram of one quardrant in the r-θ plane showing the locations of the components of the HCAL: HB, HE, HO and HF, with lines of constant η shown.

of scintillators on the outside of the coil, known at the HCAL Outer (HO). This provides shower containment in the central region, where the number of interaction lengths travelled by a particle is at its lowest [9].

The barrel consists of two halves each with 18 identical azimuthal wedges, extending outwards 0.96m. Each wedge has 17 layers of 3.7mm thick plastic scintillator, interspersed with brass absorber plates, with the exception of the innermost and outermost absorbers, made from stainless steel to add structural stability. Directly behind the ECAL is placed the first active layer, with more than double the scintillator thickness (9mm) to actively sample the articles traversing the support material between the ECAL and HCAL. The final layer also has this thickness to catch showers that form late in the absorber.

A similar structure makes up the end-caps with 18 wedges in ϕ containing 19 active plastic scintillators with brass absorbers between. The number of interaction lengths travelled by particles in the HB and HE is dependent on the η of the particle, and while it is 10 at high η, in the central region this is as low as 5. In order to compensate for this, an outer barrel detector is added, consisting of two layers of scintillating material outside the magnet, and therefore utilising the core as an absorber. This extends the total thickness of the full calorimeter to at least 11.8 interaction lengths.

The design of the forward calorimeters is driven by the need for radiation

hardness, as the region closest to the beam line has an energy density up to seven times greater than in the central region. Thus absorbers made of stainless steel and active scintillators of quartz fibres are chosen. Twelve ϕ wedges are located 11.2m from the point of interaction, with the fibres parallel to the beam.

Measurements of hadron energies in the region $|\eta| < 3.0$ rely not only on the HCAL setup described, as a significant fraction of hadrons with have begun to shower while travelling through the ECAL, which contributes around one interaction length. The hadronic component of these showers will continue on into the HCAL, but much of the initial electromagnetic activity ca be contained in the ECAL, thus use of measurements in both calorimeters are combined to reconstruct the true energy of a hadron. Using test beams over a range from 2 to 350 GeV/c the resolution for the reconstruction of hadron energy for the HCAL and ECAL combined is given by the following equation [10].

$$\left(\frac{\sigma}{E}\right)^2 = \left(\frac{84.7\%}{\sqrt{E}}\right)^2 + (7.4\%)^2 \tag{2.4}$$

2.2.6 Muon System

Interleaved in the iron return yoke of the detector are the components of the Muon System (MS), an important design feature giving CMS its middle initial. Many new physics signatures at high energy have final states with high momentum muons, and therefore accurately measuring these is crucial for many analyses, including Higgs and SUSY channels. As muons have high mass they interact little in the calorimeters, and thus retain a high percentage of their energy by the time they reach the iron return yoke. Putting the MS here far away from the interaction point allows finer precision, utilising the high magnetic field to bend even high momentum muons, and measuring the bending angle.

Muon momentum resolution using the MS is dominated at low energies ($0 < p_T^\mu < 200$ GeV/c) by the multiple scattering that occurs in the material prior to the first muon station, and therefore a better resolution could be obtain during the tracking system. However, it is possible to use the muon trajectory after the yoke to extrapolate back to the interaction point. Using the tracker and muon system together improves identification and measurements, especially as any particle detracted in the MS is expected to be a muon, as other particles are stopped earlier in the detector [11].

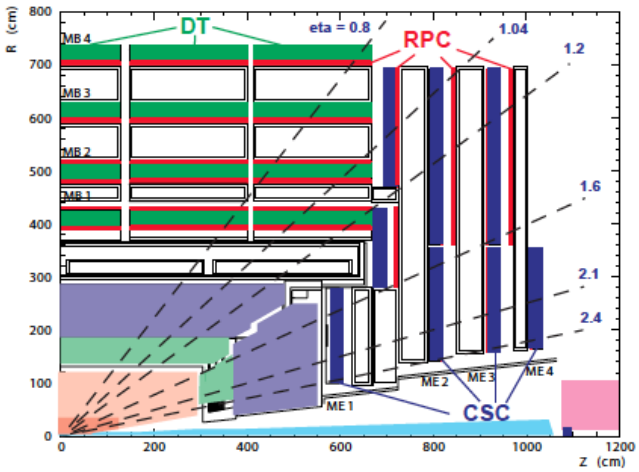

Figure 2.6: The Muon system shown in the $r - \theta$

Built within the iron yoke the MS shares the same structural layout, constructed in five barrel wheels, and two end-caps, together covering the region $|\eta| < 2.4$. As a large area must be covered, a silicon based setup such as the inner tracker would be too expensive, hence gaseous detectors are chosen. In the barrel region ($|\eta| < 1.2$) Drift Tubes (DT) are used, and in the end-caps ($0.9 < |\eta| < 2.4$) Cathode Strip Chambers (CSC) are preferred. While the DT and CSC detectors have a good position resolution, they have a long response time and are not suitable for use with the trigger, and so a third element is added in both regions, the Resistive Plate Chambers (RPC). The arrangement of the muon system is shown in Figure 2.6, with the locations of each type of detector shown.

In the barrel, the magnetic field is uniform, and therefore allows the use of Drift Tube chambers. Each of the five wheels are made up of 12 sectors, containing four chambers apiece, making up a full barrel of 240 chambers. The inner three chambers consist of three Super Layers (SL) using the first and third for the ϕ coordinate measurement and the second for the z coordinate. In the outer chamber, there are only two SL's and these contribute only to the ϕ measurement. Four layers of drift tubes make up a SL, and each layer is shifted by half a cell from the one beneath, to ensure any particle trajectory meets some active material. Each tube contains an anode wire and cathode strips, and is filled with a gas mixture of 85% Ar and 15% CO_2 gas. The Ar atoms are ionised by a

charged particle, and the resulting electrons and ions drift towards the anode and cathodes. Electrons reaching the wire are extremely excited by the high density field, which allows them to ionise further molecules, known as the "avalanche effect". Thus an electrical signal can be measured. The drift distance is 21mm and the drift time is limited to 380ns by the gas chosen, corresponding to 16 bunch crossings hence these are not suitable to provide accurate bunch information to the trigger.

Due to the aforementioned solenoidal magnetic field, the end-caps experience an irregular magnetic field, and a higher expected particle flux, and therefore drift tubes are not suitable. In this region 468 Cathode Strip Chambers are used, set out perpendicular in four stations in each end-cap. Trapezoidal chambers consist of seven radially oriented cathode strips, and in between six planes of azimuthal anode wires. The gas filling the gaps is made up of 40% Ar, 50% CO_2 and 10% CF_4, and the chambers work much in the same way as the DT's, with a high voltage applied to achieve the "avalanche effect". As the wires and strips are almost perpendicular its possible to make a simultaneous measurement in r and ϕ by identifying the charge fraction in several cathode strips.

In addition, a complimentary system of RPC's is installed in both the barrel and end-cap regions, providing extra information in the region $|\eta| < 1.6$. In the barrel there are 480 rectangular RPC's, with two layers per station, the inner two stations have one inside and one outside the DT's, and the outer two stations having both inside. The end-caps have overlapping trapezoidal chambers in the outer two concentric rings. These parallel-plate gaseous detectors have two thin gaps between plates, which are attached to high voltage to drive avalanche mode. The avalanche reaches the plates quickly, as the gas gaps have a small width, and so the measurement is made within ns, much smaller than the bunch crossing. The position resolution is adequate at the same time, and so the RPC's are used to contribute to the trigger, and also to map identified muons to a particular bunch crossing.

2.2.7 Trigger

When running at design luminosity, the LHC will collide protons with a bunch crossing of 25ns, each of which will result in 20 interactions corresponding to a rate of 40MHz of data, or 40 TB/second [12]. Not only is it impracticable for this

volume of data to be stored, but much of this corresponds to unwanted events, where no new particles have been produced, as the cross-sections for interesting physics processes are several magnitudes lower than the inelastic p-p cross section. Hence these events must be whittled into those which it is worthwhile to store and consider, which is done by the trigger system. This is divided into two components, the online hardware-based Level 1 Trigger (L1) to reduce the rate to that which can be routed from the buffer to the computing farm, and then the offline software-based High Level Trigger (HLT).

The L1 trigger is driven by the amount of time that data at the incoming rate that can be stored in the buffer, before needing to be overwritten. At design luminosity this is 128 bunch crossings, 3ns. Within this time the rate must be lowered to 10kHz, the acceptable rate for writing to the computing farm used for the HLT. This is accomplished using a tree system of triggers. First, the Regional Calorimeter Trigger (RCT) and Regional Muon Trigger (RMT) undergo local reconstruction of objects (muons, electrons, photons, jets). The Global Calorimeter Trigger (GCT) and the Global MUon Trigger (GMT) receive these objects, and sort them using a number of criteria e.g. Energy, momentum, quality of identification. The top four of each type are sent to the Global Trigger, which uses this information along with global event measurements such as total momentum to decide if the event passes an L1 Trigger requirement. If so it is sent to the HLT, if not it is not stored and passes out of the buffer.

The HLT essential does the same thing as the L1 trigger, but is not driven by strict time requirements. Running on a large computer farm of multi-core computers, it has access to the entire readout data, and performs sophisticated calculations akin to those performed in physics analyses. Using partial reconstruction algorithms to clearly identify what objects are in an event, it is possible to filter according to a set of desired physics criteria. The desired rate to store to tape is 100Hz, and the HLT is designed and monitored constantly during data-taking to ensure the correct rate is achieved. In a given run a "menu" of different trigger paths is included, to select different types of event and with different thresholds. Some require the presence of a certain object, such as a Muon. Others combine requirements, and these are called Cross-Triggers. For example a family of triggers exist that require a certain HT and MHT. Within this family there are several different thresholds, which go down as low as can

be included in the menu without raising the rate prohibitively much. Thresholds that have a rate which is too high become "pre scaled"

Chapter 3

Searching for Supersymmetry with α_T in all-hadronic events

The analysis presented here represents a model-independent search for new physics in the all-hadronic channel. Designed to search for signs of supersymmetry whilst remaining sensitive to other new physics models, the strategy centers around a selection of events which fit a topology of heavy new particles pair-produced in p-p collisions, which decay through a chain with an end product which is stable and undetectable. This is achieved in the detector by identifying several jets with a large quantity of missing energy.

3.1 Monte-Carlo Samples

3.2 Trigger

In order to select the signal events and minimise the contamination from backgrounds, a set of selection criteria is applied. As described previously in Section TRIGG, data collected by the CMS detector is stored and organised according to the L1 and HLT trigger paths passed. Each given dataset then undergoes the offline event reconstruction described in Chapter RECON/IDEN, after which n-tuples are constructed from which we apply cuts on objects and analysis variables.

Previous incarnations of this analysis for the 2010 dataset REFF used a set of pure $H_T$triggers, however these are unsuitable for the 2011 analysis as these

have too high thresholds for the analysis due to the increase in instantaneous luminosity. The use of cross-object triggers is now employed, requiring events that pass thresholds in both $H_T$and $\not{H}_{\mathrm{T}}$ for the signal region, and using the lowest un-prescaled thresholds available to ensure signal yields are accurate. As this analysis makes use of those events which fail the selection criteria also, the hadronic control sample, the pre-scaled $H_T$triggers are still used taking into account the pre-scaled factors. In the muon control sample, due to the low p_{T}threshold we use the same triggers as for the hadronic signal sample, and the photon sample makes use of the single photon trigger paths.

Having passed one of the un-prescaled triggers the events are subjected to a series of cuts on objects and analysis variables in order to select the event topologies required and minimise the background contamination.

3.2.1 Pre-Selection

The events selected must be identified as good events from the CMS detector, using a pre-selection. It is required that events have at least one good primary vertex that is not fake, with N_{dof} ¿ 4 and a vertex position along he beam axis of —z_{vtx}— $<$ 24 cm and perpendicular to the axis of ρ ¡ 2 cm. Events that have many fake tracks are identified as monester events and removed, by requiring that the ratio of High Purity tracks to the total number be greater than 25% in events with more than 9 tracks.

Events where noise has been identified in the HCAL are removed also, using an algorithm which checks for Photodetectors which have at east 17 out of 18 channels with an E ¿ 1.5 GeV.

Events are then selected according to the following preselection:

- Require events with $\mathrm{N}_{jet} \geq 2$
- N_{muon}, $\mathrm{N}_{electron}$, $\mathrm{N}_{photon} = 0$ where $p_{\mathrm{T}\mu,e} \geq 10$ GeV, $p_{\mathrm{T}\gamma} \geq 25$ GeV
- $H_T \geq$ 275 GeV
- To protect the quantity α_{T} from the scenario where many jets exist below the momentum acceptance threshold, the missing energy variable $\not{H}_{\mathrm{T}}$ estimated from jet measurment is compared to the quantity $\not{E}_{\mathrm{T}}$ measured

from the calorimters. If the ratio $R_{miss} = \not{H}_T / \not{E}_T > 1.25$, the event is rejected.

3.2.2 Object Requirements and Vetoes

Jets

Muons

Electrons

Photons

CutFlow

3.2.3 Trigger

3.3 Data to Monte-Carlo Comparisons

3.3.1 Dependence of R_{α_T} on H_T

3.4 Data-Driven Background Estimation

3.4.1 Total background prediction

3.4.2 Estimating EWK background using high p_T using W+Jets events

Types of decay contributing to Muon Control Sample

3.4.3 Estimation Z $\nu\bar{\nu}$ + jets background using photon + jets events

3.5 Systematic Uncertainties

3.6 Simultaneous Fit

3.7 Limits

3.8 Conclusion

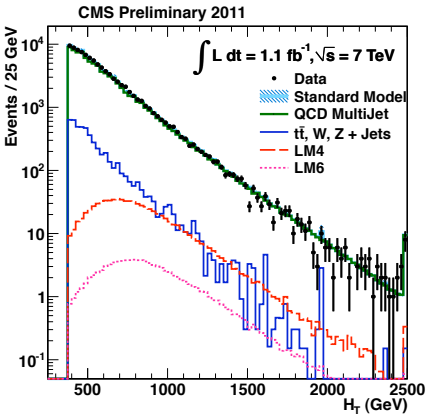

(a) Comparison of H_T between data and MC for the hadronic selection for $H_T \geq 375$ GeV and MHT > 100 GeV.

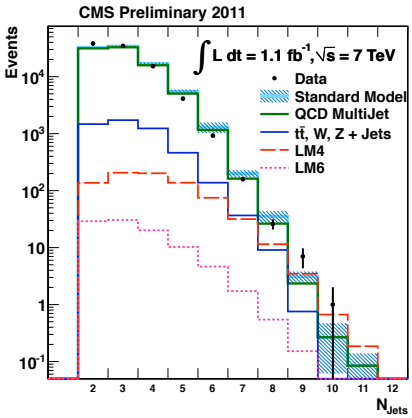

(b) Comparison of the jet multiplicity between data and MC for the hadronic selection, for $H_T \geq 375$ GeV and MHT > 100 GeV.

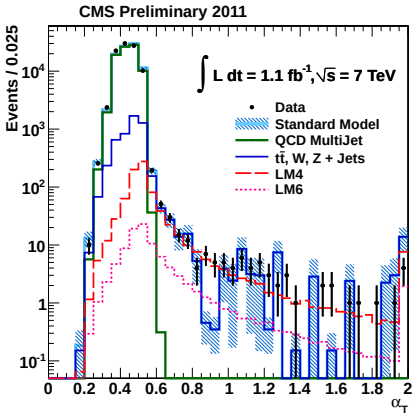

(c) Comparison of the α_T distribution between data and MC for the hadronic selection, for $H_T \geq 375$ GeV and MHT > 100 GeV.

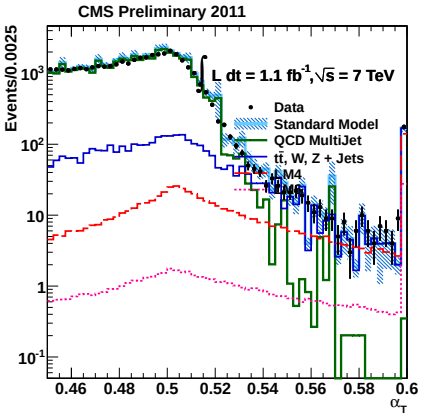

(d) Comparison of the α_T distribution highlighting the agreement on the sharply falling edge between Data and Monte Carlo for the hadronic selection, in the region $H_T \geq 375$ GeV.

Figure 3.1: Comparisons of 1.1 fb^{-1}2011 7TeV CMS Data and equivalently weighted Monte-Carlo in basic kinematic quantities prior to the α_T selection cut.

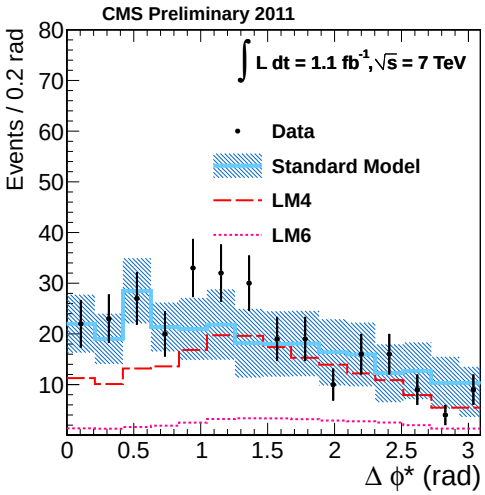

(a) $\Delta\Phi^*$ distribution after α_T selection.

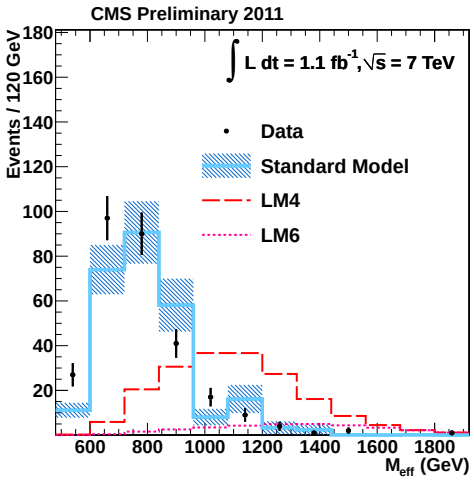

(b) The effective mass distribution, $M_{\text{eff}} = H_T + \text{MHT}$, of the events passing the α_T selection.

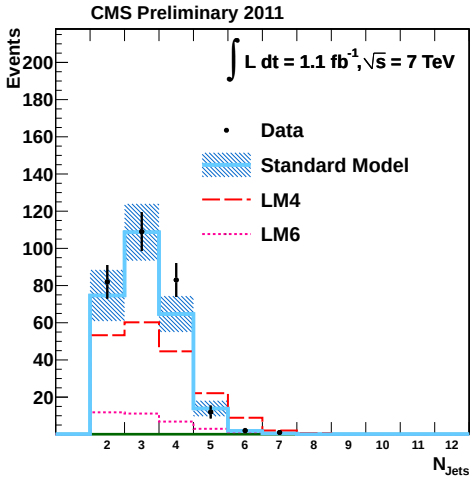

(c) Jet multiplicity after α_T selection.

Figure 3.2: Comparisons of 1.1 fb^{-1}2011 7TeV CMS Data and equivalently weighted Monte-Carlo in basic kinematic quantities after the α_T selection cut.

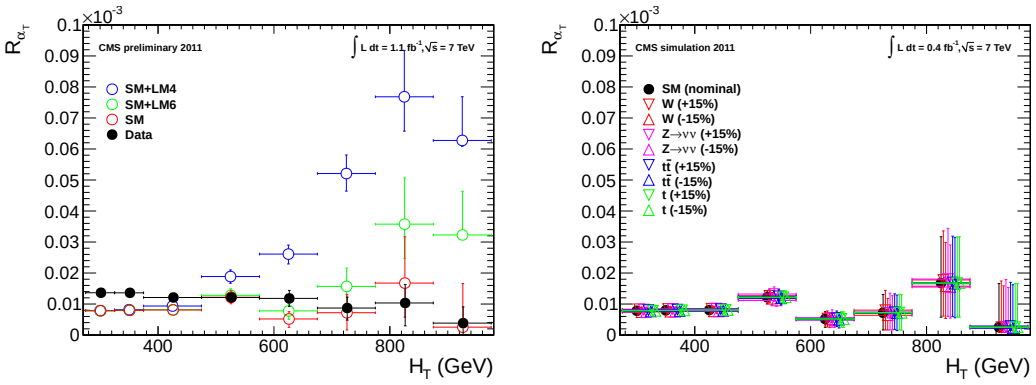

Figure 3.3: (Left) The dependence of R_{α_T} on $H_T$for events with $N_{jet} \geq 2$. (Right) Dependence of rat on $H_T$when varying the effective cross-section of the four major EWK background components individually by $\pm 15\%$. (Markers are artificially offset for clarity.)

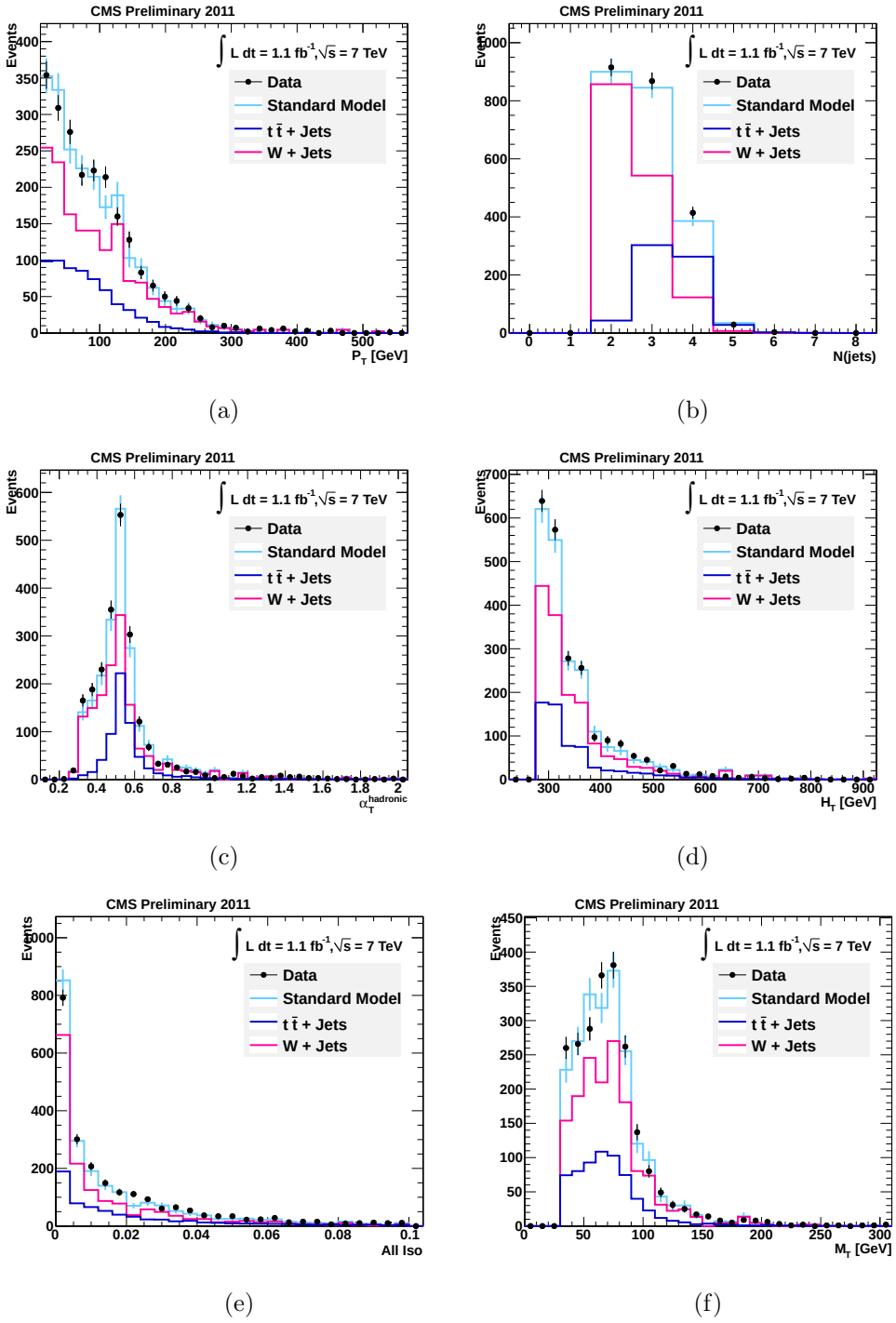

Figure 3.4: Data - Monte Carlo comparisons for the muon control selection before the $\alpha_T > 0.55$ cut is applied, shown for (a) α_T and (b) H_T, (c) Muon Combined Isolation and (d) M_T. A cut of HT >375 GeV has been applied, to select the region of fixed jet thresholds.

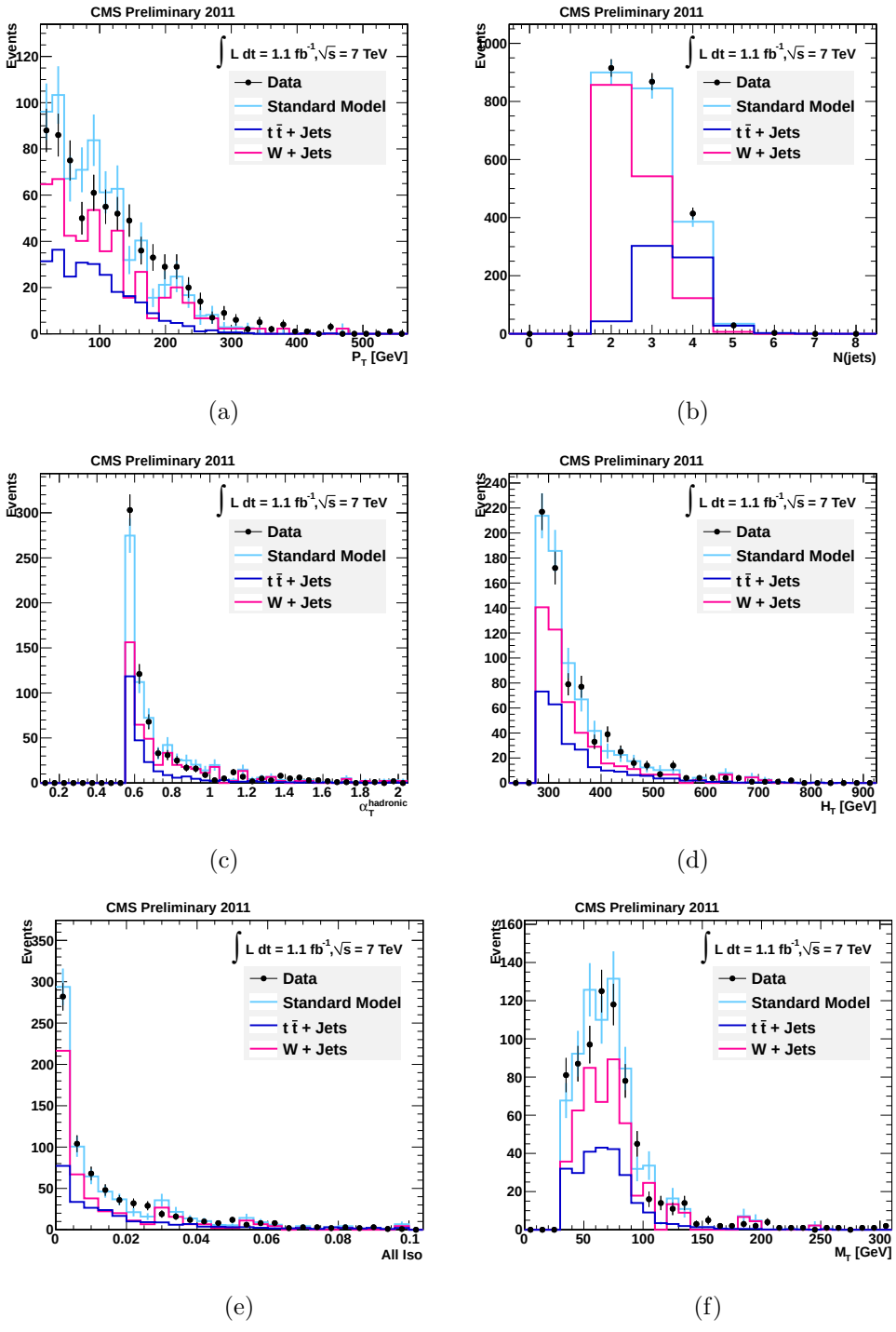

Figure 3.5: Data - Monte Carlo comparisons for the muon control selection after the $\alpha_T > 0.55$ cut is applied, shown for (a) H_{T} and (b) M_T, (c) Muon Combined Isolation and (d) M_T. A cut of HT >375 GeV has been applied, to select the region of fixed jet thresholds.

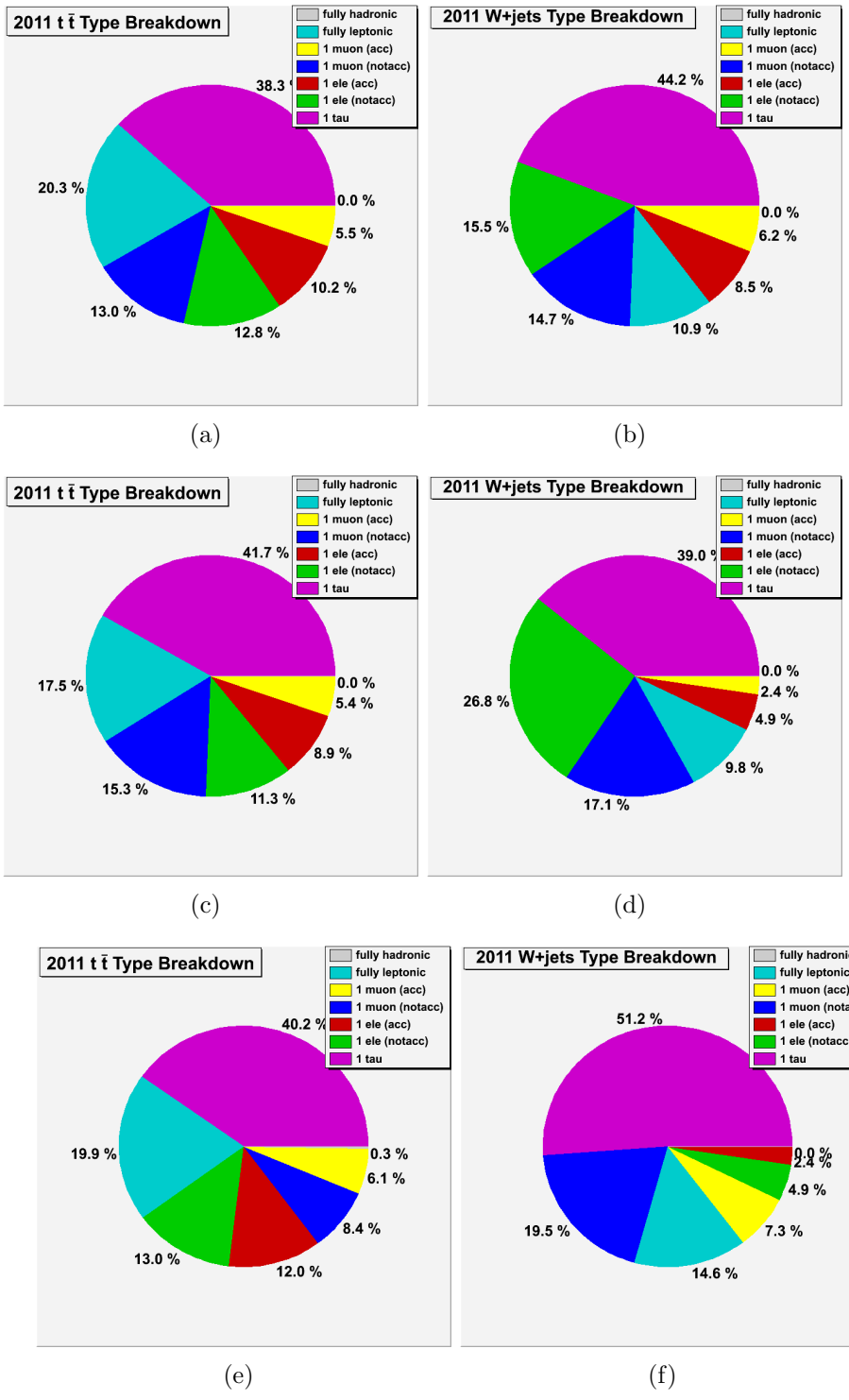

Figure 3.6: Type breakdown of decays resulting in an event selected by the Muon Control selection, shown using Monte-Carlo truth information separately for $t\bar{t}$ + jets (left) and W + jets (right) events. The breakdown is made separately for each jet-scale case: 275 $<H_T<$325 GeV (top), 325 $<H_T<$375 GeV (middle), and $H_T>$375 GeV (bottom).

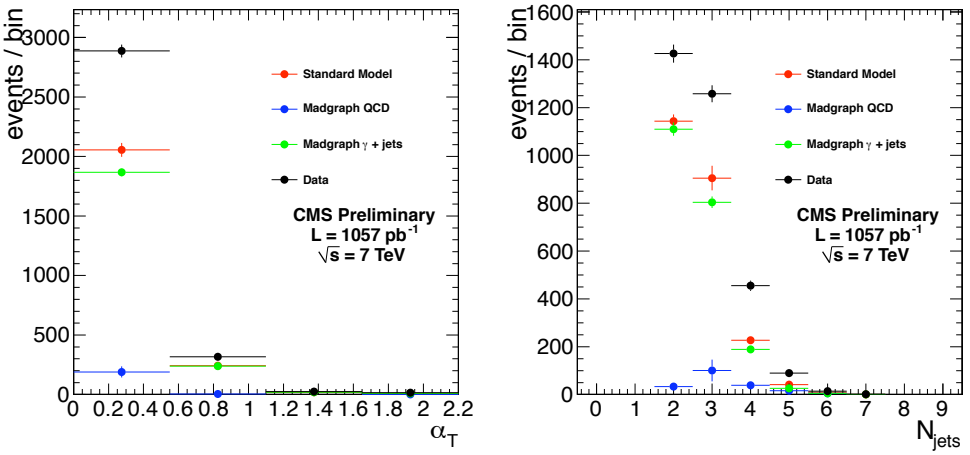

(a) (b)

Figure 3.7: Data-MC comparisons for the photon control sample. $H_{\mathrm{T}} > 375$ GeV and $\not{H}_{\mathrm{T}}/H_{\mathrm{T}} > 0.4$ are required. Left: the distribution of α_T. Right: the distribution of the number of jets.

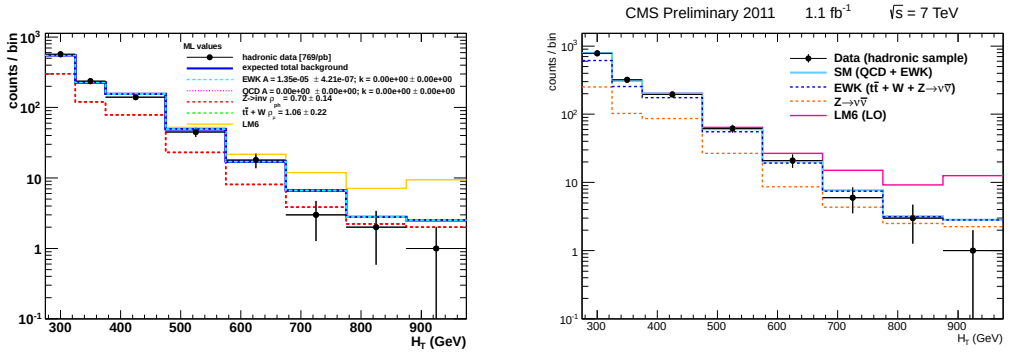

Figure 3.8: H_{T} distribution for events in the hadronic signal sample for scenario a) (left) and scenario b) (right). Shown are the events observed in data (black points), the outcome of the fit (blue line) and a breakdown of the individual background contributions as predicted by the control samples. A possible signal contribution from benchmark point LM6 is indicated as well (yellow line).

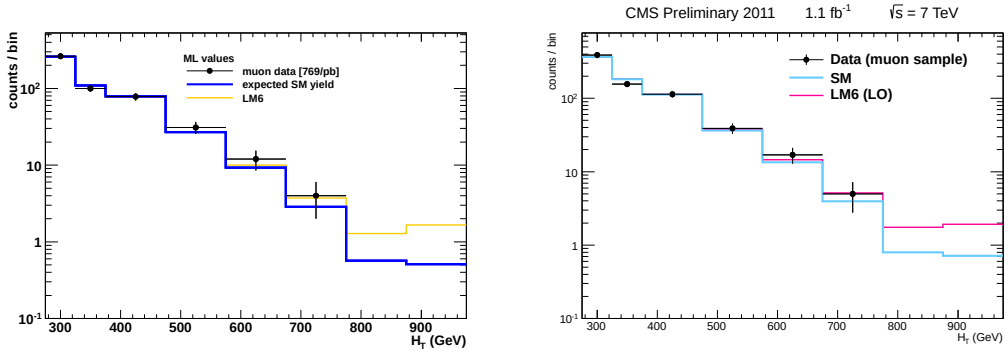

Figure 3.9: H_{T} distribution for events selected in the muon control sample for scenario a) (left) and scenario b) (right). Shown are the events observed in data (black points), the outcome of the fit (blue line) and the MC expectation (dashed line). A possible signal contribution from benchmark point LM6 is indicated as well (yellow line).

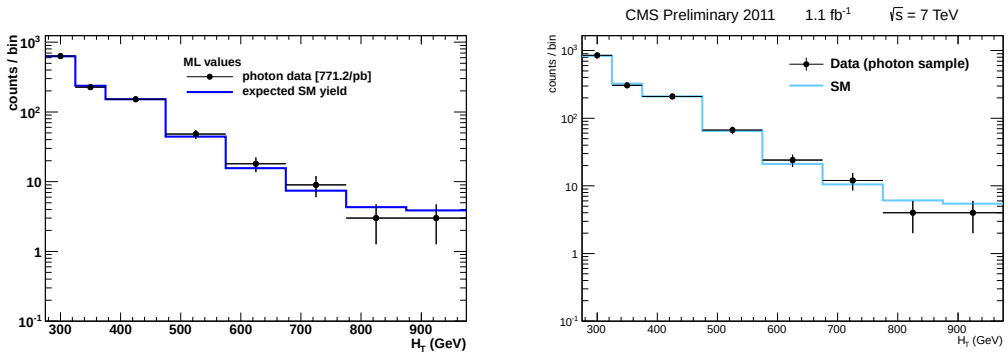

Figure 3.10: H_{T} distribution for events selected in the photon control sample for scenario a) (left) and scenario b) (right). Shown are the events observed in data (black points), the outcome of the fit (blue line) and the MC expectation (dashed line).

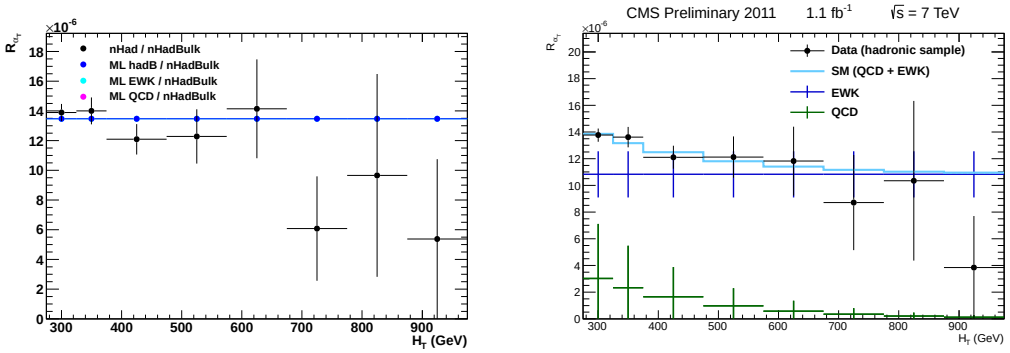

Figure 3.11: R_{α_T} as a function of H_T as observed in data (black points) and the results of the fit assuming different scenarios: a) (left) and b) (right) .

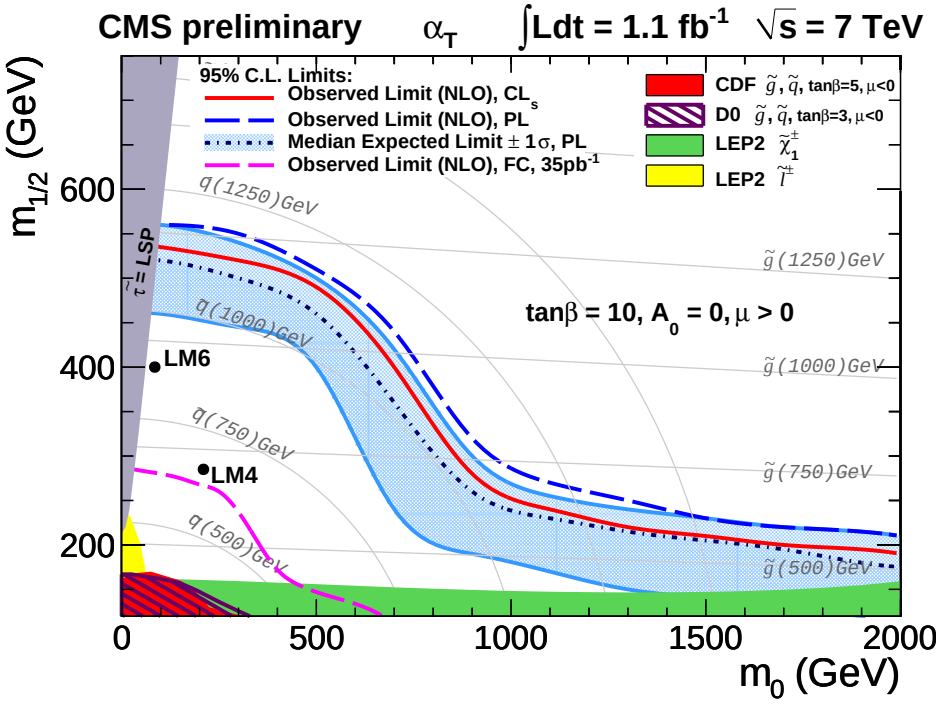

Figure 3.12: Observed and expected 95% CL exclusion contours in the CMSSM $(m_0, m_{1/2})$ plane $(\tan\beta = 10, A_0 = 0, \mu > 0)$ using NLO signal cross sections using the Profile Likelihood (PL) method. The expected limit is shown with its 68% CL range. The observed limit using the CL_s method is shown as well.

Bibliography

[1] S. L. Glashow. Partial Symmetries of Weak Interactions. *Nucl. Phys.*, 22:579–588, 1961.

[2] Jeffrey Goldstone, Abdus Salam, and Steven Weinberg. Broken symmetries. *Phys. Rev.*, 127:965–970, Aug 1962.

[3] Benjamin W. Lee, C. Quigg, and H. B. Thacker. Weak interactions at very high energies: The role of the higgs-boson mass. *Phys. Rev. D*, 16:1519–1531, Sep 1977.

[4] F. Zwicky. Die Rotverschiebung von extragalaktischen Nebeln. *Helvetica Physica Acta*, 6:110–127, 1933.

[5] Oliver Sim Brning, Paul Collier, P Lebrun, Stephen Myers, Ranko Ostojic, John Poole, and Paul Proudlock. *LHC Design Report*. CERN, Geneva, 2004.

[6] Thomas Sven Pettersson and P Lefvre. The Large Hadron Collider: Conceptual Design. Technical Report CERN-AC-95-05 LHC, CERN, Geneva, Oct 1995.

[7] The CMS Collaboration. The Compact Muon Solenoid Technical Proposal. *CERN/LHCC*, 94-38, 1994.

[8] K et al. Nakamura. Review of particle physics, 2010-2011. review of particle properties. *J. Phys. G*, 37(7A):075021, 2010. The 2010 edition of Review of Particle Physics is published for the Particle Data Group by IOP Publishing as article number 075021 in volume 37 of Journal of Physics G: Nuclear and Particle Physics. This edition should be cited as: K Nakamura et al (Particle Data Group) 2010 J. Phys. G: Nucl. Part. Phys. 37 075021.

[9] The CMS Collaboration. *The CMS hadron calorimeter project: Technical Design Report*. Technical Design Report CMS. CERN, Geneva, 1997.

[10] Efe Yazgan. The CMS barrel calorimeter response to particle beams from 2-GeV/c to 350-GeV/c. *J. Phys. Conf. Ser.*, 160:012056, 2009.

[11] The CMS Collaboration. *The CMS muon project: Technical Design Report*. Technical Design Report CMS. CERN, Geneva, 1997.

[12] Sergio Cittolin, Attila Rcz, and Paris Sphicas. *CMS trigger and data-acquisition project: Technical Design Report*. Technical Design Report CMS. CERN, Geneva, 2002.